Small scale dynamics of isotropic viscoelastic turbulence

Minh Quan Nguyen, Alexandre Delache, Serge Simoëns, Wouter J.T. Bos, Mahmoud El Hajem

Small scale dynamics of isotropic viscoelastic turbulence

M. Quan Nguyen,[1,*] Alexandre Delache,[2] Serge Simoëns,[1]
Wouter J. T. Bos,[1] and Mamoud El Hajem[1]
[1]*LMFA–CNRS UMR5509–Ecole Centrale de Lyon, Université Lyon 1, INSA de Lyon, France*
[2]*LMFA UMR 5509 CNRS–site de Saint-Étienne, Université de Lyon,*
Université Jean Monnet de Saint-Étienne, France
(Received 13 January 2016; published 14 December 2016)

The comparison of the results of direct numerical simulations of isotropic turbulence of Newtonian and viscoelastic fluid provides evidence that viscoelasticity modifies qualitatively the behavior of the smallest scales: we observe a power law in the far dissipation range of the fluid kinetic energy spectrum and we show that it is a robust feature, roughly independent of the large scale dynamics. A detailed analysis of the energy transfer shows that at these scales energy is injected into the fluid flow through polymer relaxation. It is further shown that a part of the total energy is transferred among scales through an interaction of the velocity field with the polymer field.

DOI: 10.1103/PhysRevFluids.1.083301

I. INTRODUCTION

The presence of a small quantity of polymer in a Newtonian solvent can create spectacular changes in the drag experienced in channels or pipes. Indeed, adding only a few parts per million of polymer molecules in a Newtonian fluid can reduce the drag by 80% (see Refs. [1–3]). This phenomenon, discovered in 1948, has obviously attracted the attention of a large number of researchers, trying to understand the fundamental interaction between the polymer and its solvent (see Ref. [4] for a review). A first theory proposed by Lumley [5] in 1969 explained part of the phenomenon by considering the interaction of the polymer with the boundary layer of a flow, neglecting the polymer-solvent interaction farther away from the wall. Later theoretical work of de Gennes [6–8] around the 1990s suggested that, under some circumstances, the polymer even at low concentration may affect the behavior of the turbulent energy cascade. In some sense, this theory revived the debate on the importance of polymer effects on homogeneous turbulence and to date no comprehensive understanding of polymer-modified isotropic turbulence seems to exist.

Even if the majority of works on drag reduction focus on pipe, turbulent channel, or boundary layer flow, it seems worthwhile to continue the investigation of statistically homogeneous and isotropic turbulence (HIT) since it is the simplest statistical realization of turbulent flow. Indeed, it seems illusive to propose a universal theory of drag reduction by polymers in turbulent flows if the simplest possible flow is not understood. The essential question of how the momentum flux to the wall is modified by the presence of polymers cannot be addressed in this framework, but the interaction between the polymers and the eddies of different sizes can be addressed in such setting without introducing the complexity caused by spatial inhomogeneity and anisotropy.

However, due to the enormous separation of scale between the polymer size and the large scales of a turbulent flow, obtaining detailed information on the fluid-polymer interaction remains a challenge for both experimentalists and numerical simulations even in such an academic setting. In particular, experimentally the difficulties are severe: the polymer will break after some time in high Reynolds number turbulent flow, and most of the important data is in the microscopic scales, inaccessible to most experimental techniques. The situation seems less dramatic for numerical simulations. The increasing computational power available for numerical simulations allows an access to all different

*minh-quan.nguyen@ec-lyon.fr

flow scales of moderate Reynolds number turbulent flow. The limitation is the correct modeling of the polymers in such flow and we will come back to this in the next section.

Despite these difficulties, a consensus about several features of the interaction of polymer and turbulent fluid flow seems to exist: when a small amount of polymer is added to a fluid, the large scales of the flow are significantly affected and the small scale structures' activity is reduced. This seems to be the case in wall-bounded turbulence [9–11], in shear-driven turbulence [12], and in isotropic turbulence [13–16]. In two-dimensional HIT, it was established [17] that polymer stretching is driven by strain dominated regions as also observed in three-dimensional (3D) channel flows [18]. Results based on shell-model simulations of HIT [19,20] show that globally, the transfer of energy goes from flow's kinetic energy towards the polymer. Nevertheless, the opposite is observed in some situations, where the energy is transferred from the polymers to the fluid, in particular at small scales. Indeed, a particular mechanism of drag reduction seems to be quite robust: polymers remove energy from vortices [10] when the torque due to the polymer stress is opposed to the rotation of the vortices [21] and polymers release some of their energy close to the wall [10]. Other results from DNS of homogeneous turbulent shear flow [22] were compared to experimental measurements in channel flow and pipe flow [23,24] where it was shown that the average Reynolds shear stress (nonexistent in HIT) and velocity fluctuations perpendicular to the wall are increasingly suppressed when the drag reduction increases.

Further studies on isotropic turbulence at high Reynolds number are reported in Refs. [14,25–29]. In particular, relevant for this study is the investigation of De Angelis *et al.* [26], who established the complete scale-by-scale equation of the interaction between polymers and fluid. The experimental results of Xi *et al.* [29] try to translate the "energy balance theory " of de Gennes and Tabor [6–8] into an "energy flux balance theory" by analysis of the kinetic energy transfer. Further progress was recently made by Valente *et al.* [28], who investigated the scale-by-scale kinetic energy flux using high resolution direct numerical simulation (DNS) and showed that the polymers remove energy from large scales which is returned to the fine-scale turbulence, where it is dissipated.

Most of these results are observed at relatively high Reynolds numbers. Another interesting flow regime is observed at very low Reynolds number but high elasticity, where the polymer solution flow is characterized by chaotic fluctuations in space and time. This regime, called elastic turbulence [30–32] is characterized by a kinetic energy spectrum following a power-law decay $E_K(k) \sim k^{-\alpha}$ with $\alpha \simeq 3.5$ and k the spatial wave number. This law persists for other configurations, for example, in a two-dimensional Kolmogorov flow [33] $\alpha \simeq 3.8$. These scaling exponents are in agreement with the theory of Fouxon *et al.* [34] who predict that $\alpha > 3$. It can be argued that in the far dissipation range, at scales where inertia is negligible with respect to viscous effects, such turbulent-elastic effects should be observable as well. This is corroborated by some recent numerical studies of moderate Reynolds number decaying isotropic turbulence. At moderate Reynolds number and high elasticity, such a coexistence of inertial turbulence and elastic turbulence was also observed in channel flow and pipe flow and was called elastoinertial turbulence (EIT) [35–37]. This type of flow is peculiar because it is found both at subcritical Reynolds numbers and well beyond the critical Reynolds number. Since EIT exists already at subcritical Reynolds numbers, it demonstrates the existence of a significant flow of energy from the polymers towards the fluid flow. The energy spectra of EIT [36] show a power law with an exponent α roughly in-between $11/3$ and $14/3$. In turbulent channel flow, the streamwise spectra of the turbulent fluctuations were found to have a power-law exponent around $\alpha = 14/3$ near the wall [38] at high Reynolds number. In the studies of HIT by Watanabe and Gotoh [39,40] the scaling exponent in the viscous-elastic range is increasing with decreasing elasticity in the approximate interval 4.1–4.6. In other numerical simulations, both for three dimensions (Pelerkar *et al.* [13]) and two dimensions (Gupta *et al.* [17]), a spectrum proportional to k^{-6} can be inferred from the energy spectra (for instance in Fig. 12 in Ref. [13] and Fig. 2 in Ref. [17]). This scaling is observed for scales smaller than the Kolmogorov scale, and for even smaller scales the elastic-turbulence scaling $k^{-3.5}$ is recovered in the 3D case [13]. However, these results are obtained for moderate Reynolds but with weak elasticity contrarily to EIT and ET. It seems that small structures are already active with very weak elasticity, in contradiction with the

consensus that polymers decrease the small scale activity, as observed in channel flow. Even though this range contains a negligible amount of kinetic energy compared to the rest of the scales, it clearly displays the effect of polymer on the solvent flow.

We think that it is important to further investigate this dissipation range behavior in order to better understand the interaction between polymer and fluid. It will be shown in this work that at these very small scales an equilibrium exists between the energy input from the polymers towards the solvent, and the solvent viscous dissipation. We will further investigate the flux of polymer energy through scales using a unique decomposition of the conformation tensor [41], similar to the decomposition introduced by Casciola *et al.* [26]. The observed results help to characterize the intricate interaction of turbulent motions at different scales and the deformation and stretching of the polymer field.

In the following we will first, in Sec. II, introduce the model we used to describe the turbulent polymer flow. We will discuss the square root formulation, numerical method, and the flow parameters. In Sec. III, we will discuss the energy budget and the dependence of the polymer energy on the Weissenberg number. In Sec. IV, we will present the energy spectra we measured in the simulated flows and we will propose scaling arguments to describe the dependence of the spectra on the different flow parameters. In particular, we will focus on the spectra of the polymer energy and on the modification of the dissipation range through the presence of polymers. Finally, in Sec. V, the different contributions to the evolution equation of the energy spectra are evaluated. We further show that there exists a particular type of cascade of the total energy (defined here by the sum of kinetic energy of fluid and elastic energy of polymer) passing from the velocity field to the polymer field at small wave numbers and being reinjected in the flow field at large wave numbers.

II. MODEL DESCRIPTION AND NUMERICAL IMPLEMENTATION

A. Macroscopic model for dilute polymer solutions

In order to study the turbulent dynamics of the polymer solution, we consider a macroscopic continuum description of the fluid-polymer interaction. The widely used FENE-P model is considered (finite extension nonlinear elastic model with Peterlin approximation). In this model, the end to end vectors of polymer chains in a flow are represented by a statistical field [42]. More sophisticated models (e.g., [40]), representing the microscopic details of the polymer chains could be considered, but would considerably limit the parameter range in this study, due to the large computational cost.

All instantaneous quantities we consider depend on space and time variables. These dependencies will be omitted whenever this does not introduce any confusion. We will also consider Fourier spectra, dependent on the wave number k. We will keep the dependence on k in the notation to clearly show when a quantity is a wave number spectrum.

In the macroscopic description we use, the statistics of the end-to-end vector $\boldsymbol{R}$ correspond to the average of the end-to-end vectors of a large number of polymers contained in a fluid particle. The important statistical quantity in the description of the polymer-fluid interaction is the second order correlation of the orientation vector $\boldsymbol{R}$, called the conformation tensor $\boldsymbol{C}^*$:

$$\boldsymbol{C}^* = C^*_{ij} = \langle R_i R_j \rangle_P, \tag{1}$$

where the operator $\langle \ldots \rangle_P$ represents a statistical average over a fluid particle. When the polymer is at rest, there is no preferential direction, so that the conformation tensor takes its isotropic form $\boldsymbol{C}^* = \boldsymbol{C}^*_0$ where

$$\boldsymbol{C}^*_0 = R_0^2 \boldsymbol{I} \tag{2}$$

with R_0 the root mean square (rms) of one component of all the end-to-end vectors inside a fluid particle at rest, $\boldsymbol{I}$ the identity matrix. In the following, we will use the normalized value of the

conformation tensor

$$\boldsymbol{C} = \frac{\boldsymbol{C}^*}{R_0^2}. \tag{3}$$

Two classical, widely used models based on this type of description are the FENE-P and Oldroyd-B models (e.g., [25,43]). These models contain the Navier-Stokes equations coupled with a dynamic equation for the polymer conformation tensor. Those models are given by

$$\partial_t \boldsymbol{u} + (\boldsymbol{u}\cdot\boldsymbol{\nabla}\boldsymbol{u}) = -\boldsymbol{\nabla} p + \nu_f \Delta \boldsymbol{u} + \left\{ \frac{\nu_p}{\tau_p} \boldsymbol{\nabla}\cdot[\mathcal{P}(\boldsymbol{C})\boldsymbol{C}] \right\} + \boldsymbol{f}, \tag{4}$$

$$\boldsymbol{\nabla}\cdot\boldsymbol{u} = 0, \tag{5}$$

$$\partial_t \boldsymbol{C} + \boldsymbol{u}\cdot\boldsymbol{\nabla}\boldsymbol{C} = \boldsymbol{C}\cdot\boldsymbol{\nabla}\boldsymbol{u} + (\boldsymbol{\nabla}\boldsymbol{u})^T\cdot\boldsymbol{C} - \frac{1}{\tau_p}[\mathcal{P}(\boldsymbol{C})\boldsymbol{C} - \boldsymbol{I}], \tag{6}$$

where $\boldsymbol{u}$ is the velocity, p the pressure divided by the fluid density, ν_f the solvent viscosity, τ_p the typical relaxation time of the polymers, and $\boldsymbol{f}$ a forcing term. The quantity ν_p is an additional viscosity due to the presence of polymers in the fluid, depending on the polymer concentration. It corresponds to the difference between the asymptotic viscosity at zero shear of the polymer solution and the viscosity of pure solvent (ν_f). The Peterlin function $\mathcal{P}(\boldsymbol{C})$ takes into account the finite length of the the polymer molecules. Indeed, physically, the quantity $\boldsymbol{C}$ should have an upper bound when all polymer molecules in a fluid particle are stretched. At this point, the polymer field cannot absorb more energy from the flow. The explicit form of the Peterlin function is [44]

$$\mathcal{P}(\boldsymbol{C}) = \frac{(L_{\max})^2}{(L_{\max})^2 - \mathrm{tr}(\boldsymbol{C})}, \tag{7}$$

where $L_{\max}$ is the upper limit of the normalized polymer extension length. The Oldroyd-B model differs from the FENE-P model by not taking into account the maximum extension. In other words, the value of $L_{\max}$ is taken equal to infinity and thereby $\mathcal{P}(\boldsymbol{C}) = 1$. From a physical point of view, for many applications of dilute polymer solution, this simplification does not significantly change the dynamics. Since the Peterlin's function is a hyperbolic function it only acts significantly when the polymers are stretched near the limit. In our simulations, we use a value $L_{\max} = 15$, which is realistic (see Balci *et al.* [41]), but still high enough to neglect its influence in the interpretation of most of the results: we stay in the linear zone of the polymer deformation where we can assume that the stretching is weak (as in Refs. [26,34,43]) and $\mathcal{P}(\boldsymbol{C}) \approx 1$. This approximation will simplify the scale by scale analysis of transfer in Sec. V A. In the following, most considerations will be done under the assumption of mild stretching and in those cases the Peterlin function will be omitted from the equations.

A difference with respect to Newtonian fluid turbulence is that the total energy is now partly contained in the polymers. Indeed, the average (the bracket $\langle\ldots\rangle$ is the average over the spatial domain when applied to quantities depending on spatial variable) of kinetic energy of the fluid is

$$e_K = \tfrac{1}{2}\langle ||\boldsymbol{u}||^2\rangle = \tfrac{1}{2}\langle u_i u_i\rangle \tag{8}$$

that can be converted into polymer energy through the stretching of the polymer chains. On average, this last energy is given by the trace of the conformation tensor

$$e_p = K_p\langle C_{ii}\rangle, \tag{9}$$

where $K_p = \frac{\nu_p}{2\tau_p}$. The total energy dissipation can also be divided into two different parts. First, the viscous energy dissipation which writes (for a statistically homogeneous flow)

$$\epsilon_f = \nu_f \left\langle \frac{\partial u_i}{\partial x_j}\frac{\partial u_i}{\partial x_j} \right\rangle, \tag{10}$$

and second, the dissipation of the polymer field

$$\epsilon_p = \frac{K_p}{\tau_p}\langle C_{ii} - 3\rangle. \tag{11}$$

A further discussion of the energy budget of the flow will be given in Sec. III.

B. Square-root formulation for the conformation tensor

Physically, the matrix $\boldsymbol{C}$ must always remain positive definite by construction [44]. But, Eq. (6) is hyperbolic and there are no terms or mechanisms that prevent this matrix from losing its positive definite character. Instead of solving Eq. (6), Balci and co-workers [41] reformulated the models in terms of the unique positive symmetric square root of $\boldsymbol{C}$. Indeed, since $\boldsymbol{C}$ is positive definite, we can write $\boldsymbol{C}$ as the square of a unique symmetric matrix

$$\boldsymbol{C} = \boldsymbol{B} \cdot \boldsymbol{B}. \tag{12}$$

Such a decomposition is called square-root formulation (SRF). Instead of solving numerically the evolution of $\boldsymbol{C}$, we replace Eq. (6) by a new equation

$$\partial_t \boldsymbol{B} + \boldsymbol{u} \cdot \nabla \boldsymbol{B} = \boldsymbol{B} \cdot \nabla \boldsymbol{u} + \boldsymbol{A} \cdot \boldsymbol{B} - \frac{1}{2\tau_p}[\mathcal{P}(\boldsymbol{B} \cdot \boldsymbol{B})\boldsymbol{B} - \boldsymbol{B}^{-1}], \tag{13}$$

with a unique antisymmetric matrix $\boldsymbol{A}$ that compensates for the nonsymmetric part of $\boldsymbol{B} \cdot \nabla \boldsymbol{u}$, so that $\boldsymbol{B}$ is necessarily symmetric. The expression of $\boldsymbol{A}$ is given by

$$\boldsymbol{A} = \boldsymbol{B}^{-1} \cdot [\boldsymbol{B} \cdot \nabla \boldsymbol{u} - (\nabla \boldsymbol{u})^T \cdot \boldsymbol{B}]. \tag{14}$$

The term involving $\boldsymbol{A}$ vanishes when we convert Eq. (13) back to Eq. (6). In Ref. [41] it is shown that the new equation (13) is strictly equivalent to the old one (6). The advantage is that, if instead of computing $\boldsymbol{C}$, we compute $\boldsymbol{B}$ and recover $\boldsymbol{C}$ by Eq. (12), then $\boldsymbol{C}$ will remain definite positive by construction. Another advantage of using the SRF is that the potential energy $K_p C_{ii}$ can now be written as a quadratic quantity. This is a conceptual advantage since in turbulence theory most theoretical and phenomenological considerations use second-order moments to describe the energy distribution over time and length scales. For instance, we will consider the polymer correlation tensor, and its spectrum, in analogy with the statistical quantities for the velocity field. We explain this with more details hereafter.

The two-point correlation tensor of a homogeneous turbulent velocity field $\boldsymbol{u}$ is defined by

$$R_{ij}^K(\mathbf{r}) = \langle u_i(\mathbf{x}) u_j(\mathbf{x} + \mathbf{r})\rangle, \tag{15}$$

where $\boldsymbol{r}$ is the separation vector between two points. The kinetic energy wave vector spectrum is obtained from this tensor by a Fourier transform

$$\delta(\boldsymbol{k} - \boldsymbol{k}')E_K^{(3D)}(\boldsymbol{k}) = \frac{1}{2}\delta(\boldsymbol{k} - \boldsymbol{k}')\int_{\mathbb{R}^3} R_{ii}^K(\mathbf{r}) e^{i\boldsymbol{k}\cdot\boldsymbol{r}} d\boldsymbol{r} = \frac{1}{2}\langle \widehat{\boldsymbol{u}}_i(\boldsymbol{k})\overline{\widehat{\boldsymbol{u}}_i}(\boldsymbol{k}')\rangle, \tag{16}$$

with $\widehat{\boldsymbol{u}}$ the Fourier transform of $\boldsymbol{u}$, $\boldsymbol{k}$ the wave vector, and $\overline{*}$ the complex conjugate of $*$. Here the average $\langle \ldots \rangle$ is an ensemble average. In isotropic turbulence, the dynamics at every time t is fully determined by a single function $E_K(k)$ of the wave number $k = |\boldsymbol{k}|$ related to the three-dimensional spectrum by the relation

$$E_K(k) = \int_{|\boldsymbol{k}|=k} E_K^{(3D)}(\boldsymbol{k})\, d\boldsymbol{k}. \tag{17}$$

Thereby, the one-dimensional integral over all wave numbers yields the kinetic energy

$$\int_0^\infty E_K(k) dk = e_k. \tag{18}$$

Analogously, we define the correlation tensor of field $\boldsymbol{B}$ in homogeneous turbulence by

$$R^p_{ijkl}(\mathbf{r}) = \langle B_{ij}(\boldsymbol{x}) B_{kl}(\boldsymbol{x}+\boldsymbol{r})\rangle. \tag{19}$$

Assuming homogeneity, we define the elastic energy spectrum in a similar way as in Eq. (16):

$$\delta(\boldsymbol{k}-\boldsymbol{k}')E^{(3D)}_p(\boldsymbol{k}) = \delta(\boldsymbol{k}-\boldsymbol{k}')K_p \int_{\mathbb{R}^3} R^p_{ijij}(\mathbf{r}) e^{i\boldsymbol{k}.\boldsymbol{r}} d\boldsymbol{r} = K_p \langle \widehat{B}_{ij}(\boldsymbol{k})\overline{\widehat{B}_{ij}}(\boldsymbol{k}')\rangle, \tag{20}$$

with $\widehat{\boldsymbol{B}}$ the Fourier transform of $\boldsymbol{B}$. In the following, we will use the one-dimensional spectrum

$$E_p(k) = \int_{|\boldsymbol{k}|=k} E^{(3D)}_p(\boldsymbol{k})\, d\boldsymbol{k} \tag{21}$$

defined such that

$$\int_0^\infty E_p(k)dk = K_p\langle C_{ii}\rangle = e_p. \tag{22}$$

These definitions are similar to the ones used in Refs. [26,43] using a L^2 formulation. The difference is that here we consider the symmetric decomposition instead of an eigenbasis decomposition.

The definitions used here fit well the concept of energy density we are familiar with. Indeed, Parseval's relation holds for each component of B_{ij}: starting from relation (20), we can easily deduce Parseval's relation between the Fourier and physical space representations of the elastic energy e_p in our domain $\mathcal{D}$ of volume V:

$$e_p = \frac{K_p}{V}\int_{\mathcal{D}} C_{ii}(\boldsymbol{x})d\boldsymbol{x} = \frac{K_p}{V}\int_{\mathcal{D}} B_{ij}(\boldsymbol{x})B_{ij}(\boldsymbol{x})d\boldsymbol{x} = \frac{K_p}{V}\int_{\mathbb{R}^3} \widehat{B}_{ij}(\boldsymbol{k})\overline{\widehat{B}}_{ij}(\boldsymbol{k})d\boldsymbol{k}. \tag{23}$$

In the following, we will discuss the details of the numerical method.

C. Numerical method and numerical setup

One of the difficulties to simulate viscoelastic fluid flow comes from the preservation of the positive definiteness of the conformation tensor $\boldsymbol{C}$ during the evolution of turbulent flow at high Weissenberg number. A popular scheme is due to Sureshkumar and Beris [45], combining an artificial diffusion with a hyperbolic polymer-evolution equation (6). This artificial diffusion may be global [46] or local [10]. The advantage of this method is its simplicity but the dynamics of the polymer at small scale is strongly affected by the artificial dissipation. Other, more sophisticated schemes use a positive definiteness preserving formulation [47], a log-conformation tensor representation [48], or a square-root conformation representation [41]. These three methods were compared and reported in Ref. [49]. We choose the SRF [41] because it combines a high accuracy (spectral precision in our case) and numerical stability with little numerical dissipation. To prevent the numerical stability to be affected by Gibbs oscillations of the determined conformation tensor, an artificial diffusion (ν_a) is added to Eq. (13). However, our value for the diffusivity is significantly smaller than in other schemes. For comparison, in their DNS of channel flow, Sureshkumar *et al.* [46] used $\frac{\nu_f}{\nu_a} \approx 0.8$ and at the high resolution, Thais *et al.* [50] used $\frac{\nu_f}{\nu_a} \approx 0.2$. Our value is in the range $1250 < \frac{\nu_f}{\nu_a} < 2500$. A simulation with zero artificial viscosity ($\nu_a = 0$) is also performed (see Appendix D) in order to quantify the effect of ν_a. Note that there exist other sophisticated methods to simulate flow with polymer without explicit diffusion such as proposed in Ref. [25] or the hybrid method developed in Ref. [39].

We solve Eqs. (4) and (13) using a parallel pseudospectral code [53] in a three-dimensional box of size 2π using periodic boundary conditions with a resolution up to 256^3 collocation points. The time integration is performed using a second-order Adams-Bashforth method. A smooth filter is applied to the quadratic terms in Fourier space before these terms are multiplied in real space. This smooth filter is a modification of the $\frac{2}{3}$-dealiasing used commonly in spectral methods and has been shown to create fewer and more localized oscillations in the solutions than the $\frac{2}{3}$ procedure [54].

TABLE I. Parameter compilation of different cases. The label S denotes a stochastic forcing [51], ABC indicates a deterministic helical forcing [52]. The difference in the freely decaying simulations (nonforcing type) is that in cases c the initial condition is a fully developed velocity field, in cases d it is a synthetic Gaussian flow field with prescribed energy distribution. The quantity β is the ratio $\beta = \frac{\nu_f}{\nu_f+\nu_p}$.

Case	Forcing type	$\nu_f \times 10^2$	ν_f/ν_a	τ_p	β
a1	S	1.25		0.5	
a2	S	1.25	1250	0.5	0.909
a3	S	2.5	2500	0.5	0.909
a4	S	1.25	1250	0.5	0.833
a5	S	1.25	1250	0.75	0.909
b1	ABC	1.25			
b2	ABC	1.25	1250	0.5	0.909
c1	None	1.25			
c2	None	1.25	1250	0.5	0.909
d1	None	1.25			
d2	None	1.25	1250	0.5	0.909

Series of simulations with different forcing schemes and a series of freely decaying flows were carried out to disentangle universal features from forcing-specific features and issues related to the initialization of the velocity and polymer field. The different cases we consider are as follows:

(i) (a1,a2,a3,a4): stochastically forced flows by applying a forcing scheme [51] to the modes with wave numbers $1.5 < k < 3.5$.

(ii) Case (b1,b2): deterministically forced using a fully helical (ABC) acceleration [52] applied to $1.5 < k < 3.5$.

(iii) Case (c1,c2): decaying from a steady state of a stochastically forced Newtonian fluid.

(iv) Case (d1,d2): decaying from a synthetic field randomly generated with the same energy distribution as case (c).

For each case we consider a flow with and a flow without polymers. The Reynolds number is moderate: the Reynolds based on Taylor's microscale $\mathrm{Re}_\lambda \approx 30$ (initial value for cases c,d, steady-state value for cases a,b) and the Weissenberg numbers based on large scale time $\mathrm{Wi}_L \approx 1$. For this value of Wi, the relaxation time of the polymers is comparable to the typical integral time scale of the turbulent flow. To resolve the very fine scales, the dissipation range is resolved with a resolution of $k_{\max}\eta \approx 5.5$. Because the non-Newtonian simulations are more time consuming than the Newtonian ones, to reach the steady state faster, we precalculated simulations of the Newtonian fluid for over 40 turnover times and use the results as initial condition for each case. For all simulations, the polymer is initially at rest by imposing $\boldsymbol{B}(x,t=0) = \boldsymbol{I}$.

In total, we report the results of 11 numerical simulations. The details of the case-specific parameters are reported in Table I. In Table II, we report some quantitative results. The values of the different quantities reported in the table correspond to the statistically steady-state values for the forced simulations. For the decaying simulations, all quantities are evaluated when the polymer energy reaches its maximum value.

Some global statistics for the simulations are presented in Table II. To analyze the features of the flow, we evaluate the box-averaged values as surrogates for the ensemble averaged quantities. The angle brackets indicate the averages over the fluid domain. All wave number integrals are evaluated as discrete sums over Fourier modes.

The characteristic quantities we evaluated are the kinetic energy e_K, polymer energy e_p, viscous dissipation ϵ_f, and polymer relaxation ϵ_p. These quantities were defined in Sec. II A. Further quantities derived from these parameters are the Kolmogorov's length scale $\eta = (\nu_f^3/\epsilon_f)^{1/4}$ and the

TABLE II. Compilation of Newtonian and non-Newtonian DNS results: for forcing cases, the value is reported is a steady state, and for decaying cases, the value is reported when the polymer's energy reaches its maximum value.

Case	e_K	ϵ_f	ϵ_p	Wi_L	Wi_η	$\frac{\langle C_{ii}\rangle}{(L_{\max})^2}$	$\sigma_{C_{ii}}$	L_K	L_p	λ	η	l_L	l_{DG}
a1	0.738	0.275						0.672		0.626	0.0516		
a2	0.678	0.216	0.0295	0.5940	2.079	6.58%	12.6	0.687	0.222	0.579	0.0548	0.164	0.0478
a3	0.592	0.272	0.0348	0.5574	1.650	4.43%	7.86	0.690	0.255	0.737	0.0870	0.184	0.0942
a4	0.678	0.205	0.0551	0.5941	2.026	6.24%	12.2	0.693	0.226	0.643	0.0555	0.221	0.0555
a5	0.673	0.226	0.0513	0.9510	3.188	15.01%	28.3	0.647	0.203	0.610	0.0542	0.168	0.0544
b1	0.470	0.1056						0.806		0.746	0.0656		
b2	0.441	0.0927	0.0105	0.4177	1.361	3.20%	5.7	0.795	0.276	0.771	0.0677	0.108	0.0531
c1	0.397	0.1616					0.781		0.733	0.0655			
c2	0.383	0.1484	0.0154	0.4378	1.723	4.06%	7.4	0.707	0.195	0.568	0.0602	0.136	0.0465
d1	0.331	0.1303						0.716		0.563	0.0622		
d2	0.320	0.1204	0.0143	0.3899	1.551	3.48%	5.0	0.725	0.204	0.577	0.0635	0.123	0.0583

Taylor's microscale $\lambda = \sqrt{(10\nu_f e_K/\epsilon_f)}$. The integral length scales of the velocity and polymer field are defined by

$$L_K = \frac{\int_0^\infty k^{-1}E_K(k)dk}{\int_0^\infty E_K(k)dk}, \quad L_p = \frac{\int_0^\infty k^{-1}E_p(k)dk}{\int_0^\infty E_p(k)dk}. \tag{24}$$

The Weissenberg number measures the ratio between a typical time scale of the velocity field and the relaxation time of the polymers τ_p. This latter time scale is well defined. The velocity time scale is not unambiguously defined. We therefore report in Table II two different Weissenberg numbers for each flow. The first one is $\mathrm{Wi}_L = \tau_p\sqrt{e_K}/L_K$, a Weissenberg number based on the integral scale, and $\mathrm{Wi}_\eta = \tau_p\sqrt{\epsilon_f/\nu_f}$, based on the viscous, or Kolmogorov, time scale. The average polymer extension normalized by the finite extension length $\langle C_{ii}/(L_{\max})^2\rangle$ is, according to Table II, under 6% except for the case (a5). The assumption of mild stretching is thus not unreasonable for most simulations. A related quantity is the standard deviation of the stretching $\sigma_{C_{ii}}$, which is also reported in the Table II. The Lumley scale [5] is defined as $l_L = \sqrt{\epsilon_f\tau_p^3}$. This scale marks the scale at which the turbulence time equals the polymer relaxation time. The polymer is significantly stretched only for scales of the order of or smaller than the Lumley scale. Another characteristic scale is the de Gennes scale l_{DG}, corresponding to the length for which the energy of the polymer equals the kinetic energy [6–8]. For scales smaller than de Gennes scale, the polymer starts to affect the flow structure. The wave number corresponding to de Gennes scale $k_{\mathrm{DG}} = 1/l_{\mathrm{DG}}$ is the intersection of kinetic $E_K(k)$ and elastic energy spectra $E_p(k)$ (see Sec. V C).

III. ENERGY BUDGET

It is insightful to write the equations for the statistical average of the energy contained in our system. We will hereto restrict ourselves to the considered cases (a) of a flow in a periodic flow domain, forced by an isotropic forcing term ($\boldsymbol{f}$). In that case, the equation for the kinetic energy writes, from (4),

$$\frac{1}{2}\partial_t\langle\|\boldsymbol{u}\|^2\rangle = -\nu_f\langle\|\boldsymbol{\nabla u}\|^2\rangle + \langle\boldsymbol{f}\cdot\boldsymbol{u}\rangle + \frac{\nu_p}{\tau_p}\langle\boldsymbol{u}\cdot(\boldsymbol{\nabla}\cdot\boldsymbol{C})\rangle, \tag{25}$$

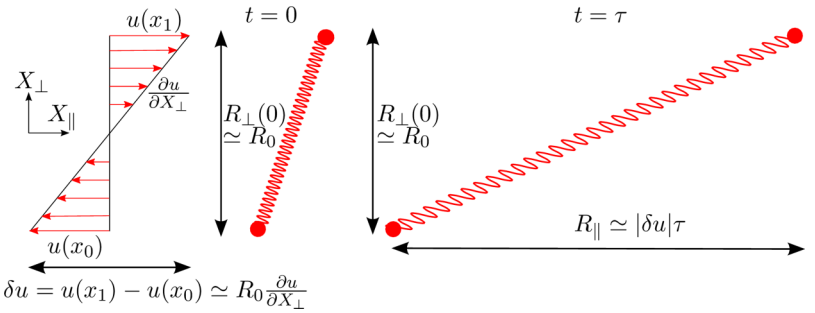

FIG. 1. Sketch of the stretching of a polymer chain by a velocity gradient during a time τ.

and the energy contained in the polymer field evolves then as

$$\partial_t \langle K_p \mathrm{Tr}(\boldsymbol{C})\rangle = -\frac{K_p}{\tau_p}\langle \mathrm{Tr}(\boldsymbol{C}) - 3\rangle + K_p \langle \mathrm{Tr}(\boldsymbol{C}\cdot\boldsymbol{\nabla u} + (\boldsymbol{\nabla u})^T \cdot \boldsymbol{C})\rangle \tag{26}$$

obtained from (6). In a homogeneous flow, we can show that the last terms of those equations are equal but of opposite sign. They therefore represent the flux of energy between the solvent and the polymer. Physically, the flow stretches the polymers, thereby injecting energy in the polymer field. Conversely, if they are properly oriented, the polymers can reinject this energy into the flow when they relax towards their equilibrium configuration.

The total energy balance equation is obtained by summing the above equations:

$$\partial_t \langle \|\boldsymbol{u}\|^2/2 + K_p \mathrm{Tr}(\boldsymbol{C})\rangle = \langle \boldsymbol{f}\cdot\boldsymbol{u}\rangle - \nu_f \langle \|\boldsymbol{\nabla u}\|^2\rangle - \frac{K_p}{\tau_p}\langle \mathrm{Tr}(\boldsymbol{C}) - 3\rangle. \tag{27}$$

In a statistically steady state, there is therefore an equilibrium between the energy injected by the random forcing on the one hand and the dissipation by viscous stresses and polymer relaxation on the other. How this energy is distributed over the two fields will be discussed now.

Intuitively, it can be understood that the extension of the polymers is determined by the relaxation time multiplied by the velocity difference between the ends of the polymer δu. This simplified picture is sketched in Fig. 1. The velocity difference can be estimated by the local velocity gradient multiplied by the end-to-end vector R_i. The projections parallel and perpendicular to the shear direction are noted $R_\parallel$ and $R_\perp$, respectively. A statistical measure for the velocity gradient in a turbulent flow is $\sqrt{\epsilon_f/\nu_f}$. Over a time τ_p, the polymer will thus be stretched to a value

$$R_\parallel(\tau_p) \approx R_\perp(0)\sqrt{\frac{\epsilon_f}{\nu_f}}\tau_p, \tag{28}$$

which is an order of magnitude estimation. If the quantity $R_\parallel \gg R_\perp \approx R_0$, it will be the value of $R_\parallel$ which will determine the trace of the conformation tensor. We have then

$$\langle C_{ii}\rangle \sim \frac{\langle R_\parallel^2\rangle}{R_0^2} \sim \frac{\tau_p^2 \epsilon_f}{\nu_f}. \tag{29}$$

This very rough estimation actually very well fits the data, as illustrated in Fig. 2. A linear fit gives

$$\langle C_{ii}\rangle = A\frac{\tau_p^2\epsilon_f}{\nu_f} = A(\mathrm{Wi}_\eta)^2, \tag{30}$$

with $A \simeq 3.3 \pm 0.2$.

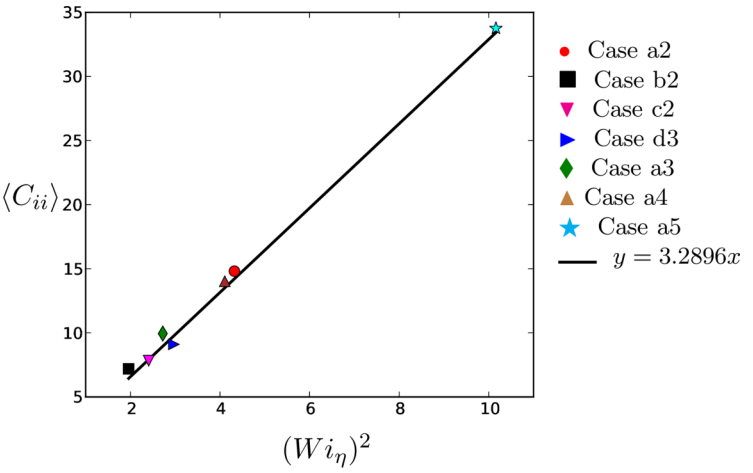

FIG. 2. Dependence of the trace of the conformation tensor on the turbulence to polymer time-scale ratio.

IV. SCALE-BY-SCALE ANALYSIS

A. Spectral energy distribution for the velocity field

The scale-by-scale energy distribution can be characterized by the kinetic energy spectrum $E_K(k)$, defined already in Eqs. (16) and (18). In Fig. 3, we show a comparison of the kinetic energy spectra as defined in Sec. II C for the Newtonian and non-Newtonian cases. Classical normalization by Kolmogorov variables is used to superpose the spectra. It is observed that the polymers do not qualitatively affect the spectrum, except in the far-dissipation range, where a power law is observed with an exponent around -6. We have performed steady-state simulations with different forcing schemes and decaying cases starting from different initial conditions. In the range of parameters we considered, the far-dissipation range power law seems to be a robust feature of the dynamics. It seems that results of Perlekar *et al.* (see Fig. 12 in Ref. [13]) and Gupta *et al.* (see Fig. 2 in Ref. [17]) support this power law. In three-dimensional simulations [13], a second power law with an exponent $\alpha = 3.5$ was found for even smaller scales. This second power law, absent in our simulations, is most probably a signature of elastic turbulence, more clearly observed in the very small Reynolds number limit [30–32]. For a given large scale Weissenberg number, the local Reynolds number,

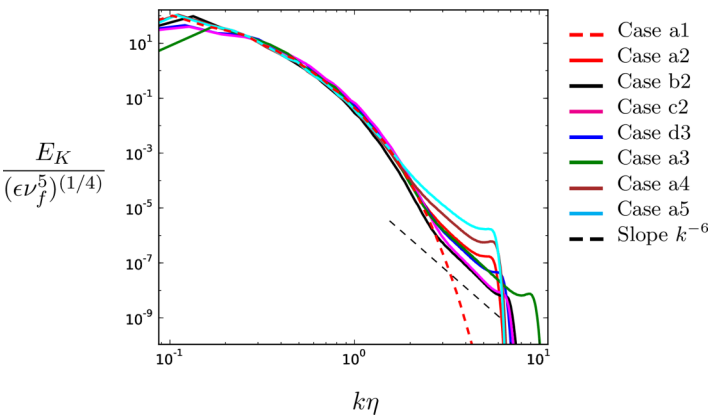

FIG. 3. Comparison of normalized fluid kinetic energy spectra E_K between non-Newtonian behavior (continuous lines) and Newtonian behavior (red dashed line).

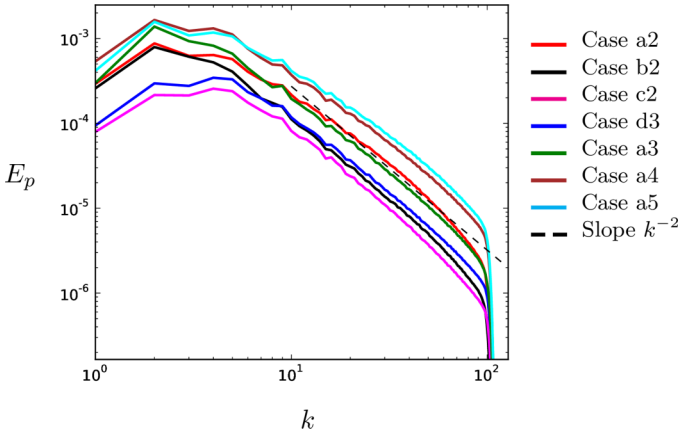

FIG. 4. Polymer energy spectra for all considered cases.

based on the scale size, decreases for large k and elastic turbulence is therefore observed in those simulations, as well as in those by Watanabe and Gotoh [39,40]. It seems that the k^{-6} power law is not a signature of elastic turbulence, but corresponds to an intermediate range where the local ratio Wi/Re is still too small to observe elastic instabilities. Indeed, it will be shown in the following that this range corresponds to an injection of energy from the polymers to the fluid flow, damped by viscous dissipation.

To confirm our results, we mildly varied three key parameters: the viscosity of the fluid ν_f, the variation of the ratio $\frac{\nu_p}{\nu_f}$, and the relaxation time τ_p around the reference case (a2). The three corresponding simulations are noted, respectively, (a3), (a4), and (a5). Figure 3 also shows the spectrum of the kinetic energy of those cases.

B. Spectral energy distribution for the polymer field

The scale-by-scale polymer energy can be represented by the elastic energy spectrum (cf. Ref. [43]), defined in Eqs. (20) and (21). In Fig. 4, we show this spectrum for all of our cases. We observe that they all obey roughly the same power law $E_p(k) \sim k^{-\gamma}$ with $\gamma \approx 2$, practically over the whole wave number range. The exponent of this power law seems to be independent of the different forcing or decay parameters and of the different flow parameters. The results of De Angelis *et al.* [43] support this finding (Fig. 6 in Ref. [43]), where we can also deduce a power-law exponent around -2. Our results are similar to those of [43] even though we use a different decomposition of the matrix $\boldsymbol{C}$ (a square-root eigenbasis decomposition in Ref. [26] versus a symmetric decomposition in this work), the two decompositions have the same physical meaning, and the polymer energy spectrum presented by De Angelis *et al.* [43] displays the same power law $E_p(k) \sim k^{-2}$. Nevertheless, in their range of high elasticity, moderate Reynolds number and high artificial diffusion $\nu_f/\nu_a = 1$, the change in slope of the kinetic energy spectrum towards a k^{-6} far-dissipation range will not be observable.

C. Scaling

Using these observations and the arguments of Sec. III, we now suggest how the scaling is determined by the different flow parameters. First of all, it seems that there is no particular length scale involved in the polymer dynamics, other than the integral length scale. Indeed, power-law scaling is observed for $E_p(k)$ between the integral scale and the smallest resolved scales. We therefore propose an *ad hoc* scaling for $E_p(k)$,

$$E_p(k) \sim e_p^F L_p (kL_p)^{-2} + e_p^M \delta(k), \tag{31}$$

where L_p is the polymer integral length scale defined in Eq. (24). The quantities e_p^F and e_p^M represent, respectively, the contributions of fluctuating and mean part of polymer elastic energy e_p:

$$e_p^F = \int_{k>0}^{\infty} E_p(k)dk = K_p\langle B_{ij}B_{ij}\rangle - K_p\langle B_{ij}\rangle\langle B_{ij}\rangle, \tag{32}$$

$$e_p^M = E_p(0) = K_p\langle B_{ij}\rangle\langle B_{ij}\rangle. \tag{33}$$

We further recall that, according to Fig. 2,

$$e_p = \int_0^{\infty} E_p(k)dk = e_p^F + e_p^M = K_p\langle C_{ii}\rangle \approx AK_p(\mathrm{Wi}_\eta)^2, \tag{34}$$

where A is the coefficient obtained by linear regression in Sec. III. Combining these expressions, we find the following scaling:

$$E_p(k|k \neq 0) \approx [A(\mathrm{Wi}_\eta)^2 - \langle B_{ij}\rangle^2]K_pL_p(kL_p)^{-2}. \tag{35}$$

The scaling exponent -2 is in this expression obtained from observation, rather than phenomenological arguments. For the moment, we have not found any convincing Kolmogorov-type or Batchelor-type arguments to further explain the scaling.

For the k^{-6} range in the dissipation range of the energy spectrum we have the following suggestion. In this range, in the Navier-Stokes equation, we expect a balance between viscous stresses and polymer relaxation:

$$-\nu_f\Delta\boldsymbol{u} \approx \left\{\frac{\nu_p}{\tau_p}\boldsymbol{\nabla}\cdot[\mathcal{P}(\boldsymbol{C})\boldsymbol{C}]\right\}. \tag{36}$$

Indeed, the other terms in Eq. (4) are expected to be negligible for $k \gg k_\eta$. Ignoring the Peterlin correction, Fourier transforming this equation and squaring both sides, we have

$$\nu_f^2k^4\frac{E_K(k)}{4\pi k^2} \approx \left(\frac{\nu_p}{\tau_p}\right)^2 k_ik_jG_{ij}(\boldsymbol{k}), \tag{37}$$

where $G_{ij}(\boldsymbol{k})$ is defined such that

$$\int_{\mathbb{R}^3} G_{ij}(\boldsymbol{k})d\boldsymbol{k} = \langle C_{im}C_{jm}\rangle. \tag{38}$$

From Eq. (37), assuming isotropy, mirror symmetry, and Gaussianity of the polymer fluctuations, we can obtain the scaling factor of $E_K(k)$ (see Appendix A):

$$E_K(k) \approx \left(\frac{L_p^3}{\nu_f^2}\right)Q_f(kL_p)^{-6}, \tag{39}$$

where the quantity $Q_f = (e_p^M)^2 + 6e_p^Me_p^F + 3(e_p^F)^2$. In order to check if our assumptions are in agreement with the dynamics of the flow, we replace Q_f by our prediction for the polymer spectrum

$$Q_f = K_p^2\{3[A(\mathrm{Wi}_\eta)^2 - \langle B_{ij}\rangle^2]^2 + 6\langle B_{ij}\rangle^2[A(\mathrm{Wi}_\eta)^2 - \langle B_{ij}\rangle^2] + \langle B_{ij}\rangle^4\}. \tag{40}$$

We will now check whether the scaling relations (35) and (39) correctly predict the results. In Figs. 5(a) and 5(b), the spectra are normalized in such a way that they should collapse if our arguments are correct. It is observed that the collapse is in general quite good. Note that the spectrum $E_K(k)$ for cases a5 and b2 are slightly off in the dissipation range. We note that case a5 is the case that corresponds to the most-stretched case and the Peterlin approximation yields a correction of approximately 25% in this case. Case b2 is the case with a fully helical forcing, but we have neglected helicity in expression (A2). Further refinement of our arguments would be required to take into account the influence of helicity or the Peterlin correction. The spectra of polymer energy collapse rather well using the proposed scaling.

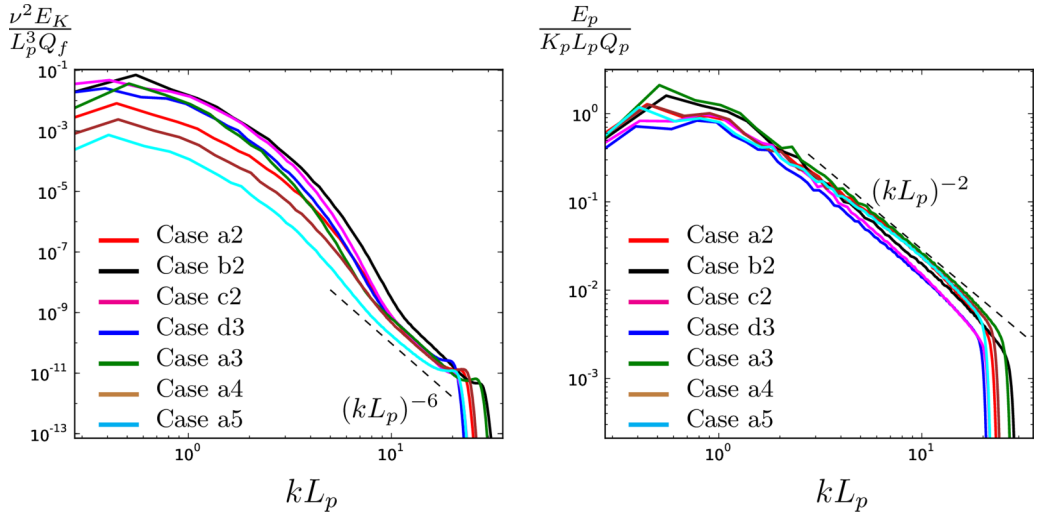

FIG. 5. Normalized spectra. The normalization is chosen such that the spectra should collapse if our scaling arguments leading to expressions (35) and (39) are correct. The factor Q_f is defined in Eq. (40) and $Q_p = A(\mathrm{Wi}_n)^2 - \langle B_{ij}\rangle^2$.

V. A SCALE-BY-SCALE ANALYSIS OF ENERGY TRANSFER

A. Lin's equation

Lin's equation describes the evolution of the kinetic energy spectrum. In the absence of polymer drag or external body forces, the equation reads as, for homogeneous turbulence,

$$\partial_t E_K(k) = T_f(k) - 2\nu_f k^2 E_K(k) + F(k). \tag{41}$$

In this equation, $T_f(k)$ is the nonlinear transfer term, responsible for the energy transfer between length scales, due to nonlinear mode coupling. The term $2\nu_f k^2 E_K(k) = D_f(k)$ is the energy dissipation spectrum and its integral yields the kinetic energy dissipation. The term $F(k)$ is the forcing spectrum. If through the forcing term sufficient energy is injected at a constant rate, the flow will become statistically stationary and the time derivative $\partial_t E_K(k)$ will tend to zero.

The Lin equation for viscoelastic turbulence was first obtained by Casciola *et al.* [26] using the square-root eigenbasis decomposition. Here, we use the square-root decomposition of matrix $\boldsymbol{C}$. First, we write Eqs. (4) and (13) in Fourier space for each wave vector $\boldsymbol{k}$ under the assumption of mild stretching $\mathcal{P}(\boldsymbol{C}) \approx 1$ (but the Peterlin correction can be taken into account properly without any difficulty, if needed):

$$\partial_t \widehat{\boldsymbol{u}}(\boldsymbol{k}) + \mathbf{P}(\boldsymbol{k}) \cdot (\widehat{\boldsymbol{u}\cdot\nabla\boldsymbol{u}})(\boldsymbol{k}) = -\nu_f \boldsymbol{k}^2 \widehat{\boldsymbol{u}}(\boldsymbol{k}) + \frac{\nu_p}{\tau_p}\mathbf{P}(\boldsymbol{k}) \cdot [\nabla \cdot \widehat{(\boldsymbol{B}\cdot\boldsymbol{B})}(\boldsymbol{k})] + \widehat{\boldsymbol{f}}(\boldsymbol{k}), \tag{42}$$

$$\partial_t \widehat{\boldsymbol{B}}(\boldsymbol{k}) + \widehat{\boldsymbol{u}\cdot\nabla\boldsymbol{B}}(\boldsymbol{k}) = \widehat{\boldsymbol{B}\cdot\nabla\boldsymbol{u}}(\boldsymbol{k}) + \widehat{\boldsymbol{A}\cdot\boldsymbol{B}}(\boldsymbol{k}) + \frac{1}{2\tau_p}[\widehat{\boldsymbol{B}}(\boldsymbol{k}) - \widehat{\boldsymbol{B}^{-1}}(\boldsymbol{k})], \tag{43}$$

where $\widehat{*}$ is the Fourier transform as defined previously and $\mathbf{P}(\boldsymbol{k})$ is the projector $[\mathbf{P}(\boldsymbol{k})]_{ij} = \delta_{ij} - k_i k_j / k^2$ subtracting the potential part of a vector field.

To obtain Lin's equation, we multiply both sides of Eq. (42) by the complex conjugate of $\widehat{\boldsymbol{u}}(\boldsymbol{k})$, and sum it with the complex conjugate of Eq. (42) that was also previously multiplied by $\widehat{\boldsymbol{u}}(\boldsymbol{k})$. Averaging this vectorial quantity over spherical shells S_k of radius k and normalizing, we obtain Lin's equation for the kinetic energy $E_K(k)$. The equation for the spectrum $E_p(k)$ is analogously

obtained from Eq. (43). We hereby have the following evolution equations for spectra of kinetic energy $E_K(k)$ and elastic energy $E_p(k)$:

$$\partial_t E_K(k) = T_f(k) - D_f(k) + S_{p\to f}(k) + F(k), \tag{44}$$

$$\partial_t E_p(k) = T_p(k) - R(k) + S_{f\to p}(k) + T_a(k) - D_a(k). \tag{45}$$

We now discuss the different contributions in these equations. First, in the evolution equation for $E_K(k)$ [Eq. (44)], only one new term appears compared to the equation for Newtonian flow [Eq. (41)]. This term is $S_{p\to f}(k)$ and represents the energy transfer from the fluid to the polymers. It is thus necessarily this term that is involved in the modification of the velocity field by its interaction with the polymers.

The second equation for the evolution of $E_p(k)$ contains five different terms on the right-hand side. Those are now discussed.

(1) The polymer-energy transfer term $T_p(k)$ represents a redistribution of polymer stress over different scales. Its integral over all wave numbers is thus zero.

(2) $R(k)$ is the dissipation of the polymer field. Its integral equals $\frac{K_p}{\tau_p}(\langle C_{ii}\rangle - 3)$.

(3) $S_{f\to p}(k)$ is the spectrum of the energy injection into the polymer field due to the polymer stretching. It is the only energy input and its integral therefore equals the value of $S_{p\to f}(k)$ in the balance for $E_K(k)$.

(4) The term $D_a(k) = 2\nu_a k^2 E_p(k)$ represents the artificial diffusion added to the equation developed in Balci [41].

(5) $T_a(k)$ is the transfer by the compensation term of the antisymmetric part of the stretching term. Its integral over all wave numbers is zero (see Appendix B).

B. Transfer of kinetic and elastic energy

We will now consider a steady state so that the time derivatives are zero. In Fig. 6, we consider the different contributions to the spectral evolution for case a2.

It is observed that, as in turbulence without polymers, the energy input by the forcing F is approximately in equilibrium with the nonlinear transfer: $F \approx T_f$. This energy is then transferred to other scales and the dissipation spectrum D_f extends from the smallest to the largest wave numbers: $D_f \approx T_f$. No scale separation is observed at this Reynolds number. The original feature, introduced by the polymer dynamics, is the polymer stress $S_{p\to f}$ that withdraws energy from all large scales up to $k\eta \approx 1.6$. For larger k, this term changes sign and it injects energy to the fluid at small scales. At these small scales, the energy injection through the recoiling of the polymers becomes dominant over the stretching which extracts energy from the flow. A recent investigation of isotropic viscoelastic turbulence [28] showed that a similar mechanism is also observed for larger values of Wi_η. At scales larger than $k\eta \approx 2.1$, it even becomes the dominant energy injection, balancing the dissipation rate $D_f \approx S_{p\to f}$. It is at these scales that Eq. (37) holds and it is also at these scales that the $E_K(k) \sim k^{-6}$ power law is observed.

In Fig. 6(c), the different terms in the evolution equation of $E_p(k)$ are investigated. A first observation is that the two last terms in Eq. (45), $D_a(k)$, $T_a(k)$, are small. These terms are from numerical origin and they will be neglected in the further discussion of the physics of the flow, as they are negligible. The two dominant terms are the polymer-stretching term $S_{f\to p}(k)$, which is the energy source in this balance, and the dissipation term $R(k)$, which almost perfectly balances the stretching term $R(k) \approx S_{f\to p}(k)$. This equilibrium leads to the power law of $E_p(k) \sim k^{-2}$. The value of the transfer term $T_p(k)$, representing the redistribution of polymer energy, is small compared to these last two terms.

Note that the energy transfer term of fluid to polymer $S_{f\to p}(k)$ is directly related, through triadic mode coupling, to the polymer to fluid transfer $S_{p\to f}(k)$, as we will show in the following. It is

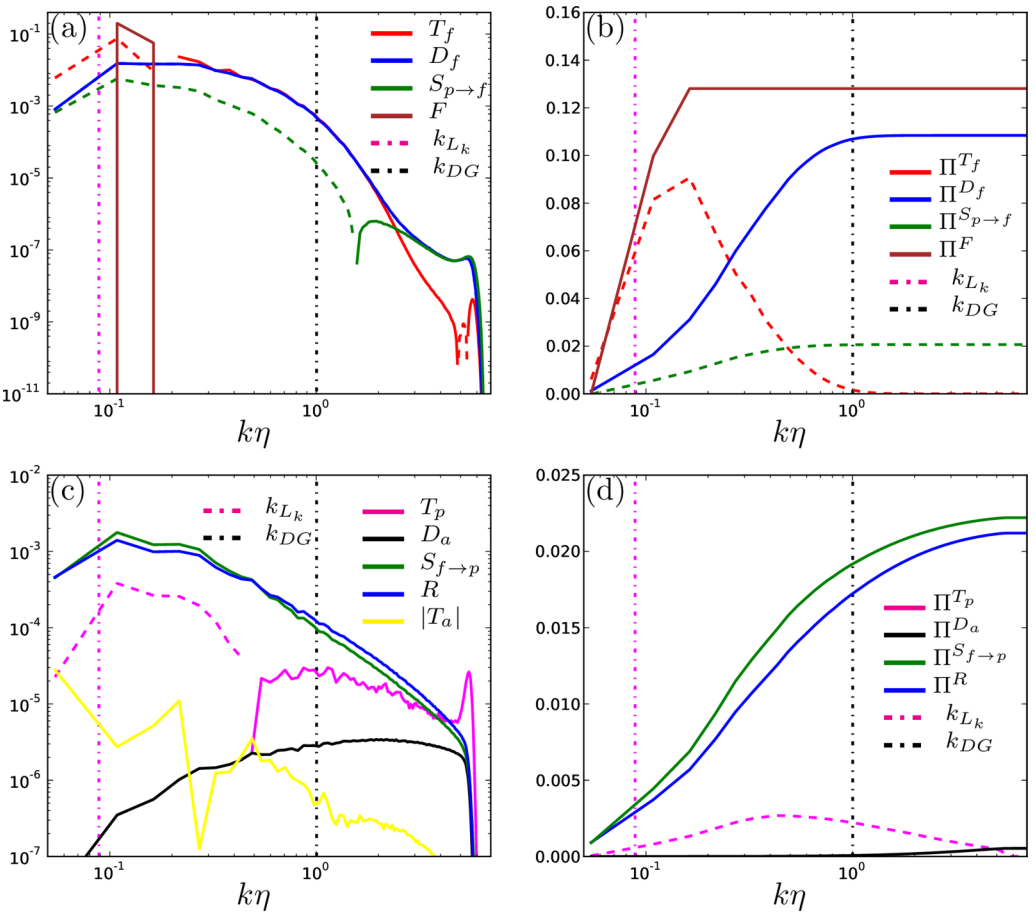

FIG. 6. (a) Different contributions in the evolution of the kinetic energy spectrum $E_K(k)$. (b) Fluxes in the kinetic energy balance. (c) Contributions in the evolution equation of the elastic energy $E_K(k)$. (d) Flux of elastic energy. In all figures, negative values are represented by a dashed line and positive values by a solid line. Vertical lines represent the velocity's integral length scale k_{L_K} and de Gennes scale k_{DG}.

also this coupling term which is responsible for the new power laws observed in the viscoelastic turbulence dynamics.

In Figs. 6(b) and 6(d), we show the different terms integrated from 0 to k. In our notation,

$$\Pi^T(k) = \int_0^k T(k^*)dk^*, \tag{46}$$

and the same convention is used for the other terms. The integrated quantities at the maximum wave number should by definition equal the terms in the average one-point energy balance (25). For example, $\Pi^F(k_{\max}) = \langle \boldsymbol{f} \cdot \boldsymbol{u} \rangle$. Indeed, we can verify the conservation of energy directly from Figs. 6(b) and 6(d). Definition (46) is particularly interesting when applied to transfer terms: for a given k, $\Pi^T(k)$ directly measures the total flux due to T from wave numbers $k^* \leqslant k$ to scales $k^* > k$. It is observed that the dominant flux in the kinetic energy balance Π^{T_f} attains a peak value of approximately 70% of the energy injected by the forcing term.

From Fig. 6(d), we observe an equilibrium in the polymer-energy budget, corresponding to (26), if we neglect the artificial diffusion. A flux of approximately 10% of the injected polymer energy is observed due to the advective transfer between scales, Π^{T_p}. The contribution of this transfer term

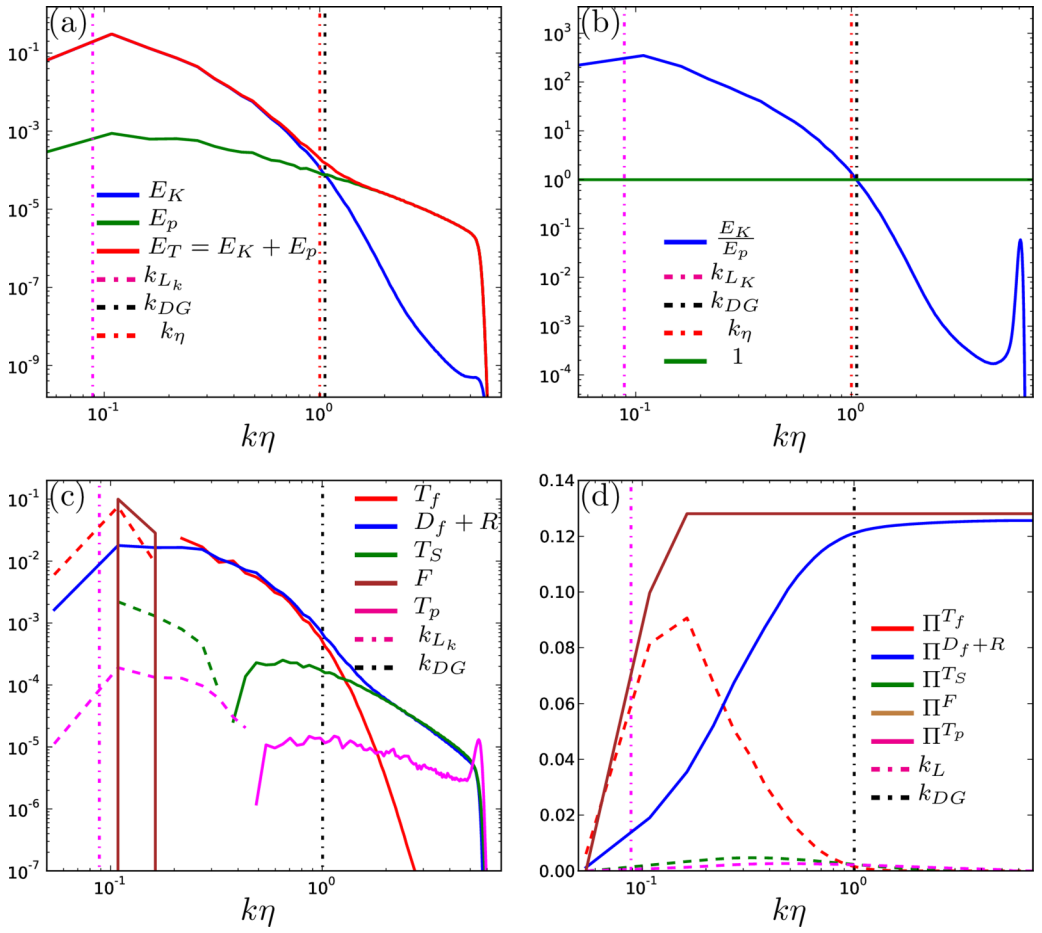

FIG. 7. (a) Components of the total energy $E_T = E_K + E_p$. (b) Ratio $\frac{E_K}{E_p}$. (c) Transfer terms for the total energy $E_T(k)$. (d) Flux of total energy. Negative values are represented by a dashed line, positive values by a solid line. The vertical lines indicate the integral length scale k_{L_K} and the de Gennes scale k_{DG}.

is small compared to the dissipation and energy input. Clearly, part of the energy injected through the forcing $\langle \boldsymbol{f} \cdot \boldsymbol{u} \rangle$ in the velocity field is transferred to the polymer field. The total amount of this transferred energy is $\Pi^{S_{f\to p}}(k_{\max})$. This energy is dissipated by the polymer dissipation, resulting in the approximate balance $\Pi^{S_{f\to p}}(k) \approx \Pi^{R}(k)$.

In Figs. 7(a) and 7(b), we have plotted the total energy E_T, the elastic energy E_p, kinetic energy E_K, and their ratio E_K/E_p, as well as the de Gennes scale k_{DG} where $E_p(k_{\mathrm{DG}}) = E_K(k_{\mathrm{DG}})$. At large scale $E_K \gg E_p$, whereas at small scale $E_K \ll E_p$.

In our case, the power law in the far-dissipation range appears approximately at $k = 2k_{\mathrm{DG}}$ which is thus slightly larger, but of the same order of magnitude as the scale where the energy balance theory of de Gennes and Tabor [6–8] predicts a modification of the velocity by polymer interaction. Note that $k = 2k_{\mathrm{DG}}$ corresponds more precisely to the scale where the transfer $S_{p\to f}$ becomes more important than the nonlinear transfer term T_f. By comparison, at higher Reynolds number, the energy balance theory of de Gennes and Tabor [6–8] suggests a two-way energy transfer between fluid and polymers at small scales. This transfer involves an overall modification of the turbulent energy cascade. Our result seems in agreement with this de Gennes picture even at low Wi and moderate Re: a two-way energy transfer occurs between polymer and fluid. Moreover, the mechanism based

on comparison of the transfer strength is in agreement with observations in a recent experimental investigation of high Reynolds number polymer flow, where an energy flux balance [29] was invoked to explain the results.

An interesting feature will appear if we consider the total energy balance, indeed, in that case a third transfer flux will show up, due to the fluid-polymer interaction. This will be shown in the next section.

C. A new cascade mechanism for the total energy

We consider the same case (a2) as in the last section, but instead of considering the kinetic and potential energy separately, we consider the sum. The average of total energy satisfies Eq. (27), which we recall here:

$$\partial_t \langle \|\boldsymbol{u}\|^2/2 + K_p \mathrm{Tr}(\boldsymbol{C})\rangle = \langle \boldsymbol{f}\cdot\boldsymbol{u}\rangle - \nu_f \langle \|\boldsymbol{\nabla u}\|^2\rangle - \frac{K_p}{\tau_p}\langle \mathrm{Tr}(\boldsymbol{C}) - 3\rangle. \tag{47}$$

Considering the sum of the Lin equation and its polymer counterpart, we have

$$\partial_t E_T(k) = F(k) - D_T(k) + T_f(k) + T_p(k) + T_S(k), \tag{48}$$

where we define the total energy spectra $E_T(k) = E_K(k) + E_p(k)$ and we have neglected the contributions of the numerical dissipation term $D_a(k)$ and the symmetrization term $T_a(k)$. In this equation, the total dissipation term is

$$D_T(k) = 2\nu_f k^2 E_K(k) + R(k), \tag{49}$$

which is the sum of the viscous dissipation of fluid energy and the relaxation of polymer energy. The transfer terms $T_f(k)$, $T_p(k)$ and the forcing term $F(k)$ already appeared in the expressions for the evolution of E_K and E_p. A new contribution is $T_S(k)$, which is defined as

$$T_S(k) = S_{p\to f}(k) + S_{f\to p}(k). \tag{50}$$

Its integral over all wave numbers is zero since this term represents a transfer of energy between the fields. The individual contributions $S_{p\to f}(k), S_{f\to p}(k)$ do, however, not sum up to zero scale by scale. If we consider the triadic interactions, this term can be written as

$$T_S(k) = \int_{|\boldsymbol{k}|=k} \left[\int_{\mathbb{R}^3\times\mathbb{R}^3} (t_{\boldsymbol{k},\boldsymbol{p},\boldsymbol{q}} - t_{\boldsymbol{q},\boldsymbol{k},\boldsymbol{p}})\delta(\boldsymbol{k}-\boldsymbol{p}-\boldsymbol{q}) d\boldsymbol{p}\, d\boldsymbol{q} \right] d\boldsymbol{k}, \tag{51}$$

where the terms $t_{\boldsymbol{k},\boldsymbol{p},\boldsymbol{q}}$ and $t_{\boldsymbol{q},\boldsymbol{k},\boldsymbol{p}}$ correspond to the triadic interactions behind $S_{p\to f}(k)$ and $S_{f\to p}(k)$, respectively. Detailed conservation is thus observed, triad per triad, for the transfer of total energy by polymer-fluid interaction, which yields the global transfer conservation $\int_{\mathbb{R}} T_S(k)dk = 0$. But, since $t_{\boldsymbol{q},\boldsymbol{p},\boldsymbol{k}}$ is not symmetric under permutation $(\mathbf{k},\mathbf{p},\mathbf{q}) \to (\mathbf{q},\mathbf{k},\mathbf{p})$, this term is nonzero. We thus have here a transfer mechanism between scales for the total energy, which adds to the terms $T_f(k) + T_p(k)$. Technical details on the derivation and energy conservation properties of (51) can be found in Appendix C.

The total energy presents two regimes on Fig. 7(a). A first regime ($k\eta < 1$) is dominated by kinetic energy. On Fig. 7(c), we plot the different terms. At large scale we observe that the dissipation of fluid and polymer is balanced by the nonlinear transfer term $T_f \approx D_f + R$ as in classical Newtonian flow. In the meanwhile, the interaction between polymer and fluid takes away a small part the total energy ($T_S < 0$ for $k\eta < 0.5$) and gives it back to the total energy at smaller scale ($T_S > 0$ for $k\eta > 0.5$).

A second regime ($k\eta > 1$) is dominated by polymer energy. At these small scales, the transfer by interaction dominates the standard nonlinear transfer ($T_f \ll T_S$ at $k\eta \approx 2$), and we have a new balance between the fluid and polymer interaction (stretch and stress) on the one hand and the dissipation of fluid and polymer $T_S \approx D_f + R$ on the other. This mechanism constitutes a new type

of transfer from large to small scale but for the total energy. The polymer transfer T_p is negligible when compared to other terms.

In Fig. 7(d), the budget of fluxes shows that all the power input is, on average, dissipated into heat by polymer and fluid as it should: $P \simeq \epsilon_f + \epsilon_p$. The precise ratio between the amount of energy dissipated by the polymers and the amount dissipated by the viscous dissipation is determined by the interaction between polymer and fluid.

VI. CONCLUSION

The present investigation focused on homogeneous isotropic turbulence advecting a small quantity of polymers at moderate Reynolds number and low elasticity. The parameters are chosen outside the range where elastic and elastoinertial turbulence are expected. We have shown that, in the range of parameters considered, the average amount of stretching, as measured by the trace of the conformation tensor, can be estimated by elementary arguments on the local rms velocity gradient and the polymer relaxation time. A more detailed investigation of the scale distribution of the kinetic and polymer energies showed that the dissipation range of the fluid kinetic energy spectrum displays a power law, proportional to k^{-6}. It was shown that this range can be explained by an injection of energy from the polymer field into the velocity field, where the energy is locally balanced by viscous dissipation. The observation of this power law was made possible by the use of an accurate numerical method necessitating very little artificial dissipation. The importance to avoid, as much as possible, the use of artificial diffusion was already suggested in Refs. [11,25].

The polymer-energy spectrum was shown to be described by a power law, proportional to k^{-2}. Taking into account that the scale depends mainly on the integral scale and that its integral value over all wave numbers is given by the trace of the conformation tensor, we suggested a way to collapse all the data. The observed power law is linked to the activity of the polymer which extends even to scales in the far-dissipation range of the kinetic energy spectrum.

The scale by scale evaluation of the different terms in the evolution equation of the kinetic energy spectrum allows to demonstrate that triadic interaction allows for the pumping of energy from the fluid flow at large scales to the polymer field, which returns a part of this energy to the fluid at small scales. In the far-dissipation range, the viscous stress balances this energy injection, and this balance leads to a k^{-6} power law in the kinetic energy spectrum. It further allows to show that scale by scale, the polymer dynamics is, to a good approximation, described by a local equilibrium between polymer stretching and relaxation. The transfer of polymer energy between scales exists but is subdominant.

Considering the total energy, i.e., the sum of kinetic and polymer energy, allows to reveal an interesting cascade mechanism involving the stretching of the polymers. Indeed, this stretching allows a transfer of energy between the fields. The interesting feature of this transfer is that the loss of kinetic energy at a given scale does not necessarily correspond to a gain of polymer energy at the same scale and vice versa. Detailed conservation of the energy of a triad allows to precisely describe this transfer.

ACKNOWLEDGMENT

The authors have benefited from discussions with Prof. Robert J. Poole. This work was granted access to the HPC resources of IDRIS under the allocation i20152a7411 made by GENCI.

APPENDIX A: SCALING OF THE k^{-6} POWER LAW IN THE KINETIC ENERGY SPECTRUM

In the wave number range where the power law $E_K(k) \approx E_K^0 k^{-6}$ emerges, we can derive the scaling factor E_K^0 by considering the equilibrium between viscous stress and polymer effects [Eq. (37)]. The tensor $G_{ij}(k)$ on the right-hand side of this equation can be written, invoking

isotropy, as

$$\langle C_{im}C_{jm}\rangle = \frac{\delta_{ij}}{3}\langle C_{mn}C_{mn}\rangle. \tag{A1}$$

In a mirror-symmetric isotropic field,

$$G_{ij}(\boldsymbol{k}) = \frac{1}{4\pi k^2}\left[a(k)\frac{k_i k_j}{k^2} + b(k)\left(\delta_{ij} - \frac{k_i k_j}{k^2}\right)\right], \tag{A2}$$

where $a(k)$ and $b(k)$ are functions of the norm of the wave vector only, not of its orientation.

The contribution of $b(k)$ will vanish when we multiply G_{ij} with $k_i k_j$. It is natural in this context to assume that $a(k)$ is a power law of k: $a(k) \sim k^{-\alpha_1}$. Using this assumption, we find that

$$G_{ij}(\boldsymbol{k}) \sim \frac{L_p\langle C_{mn}C_{mn}\rangle}{4\pi k^2}\left[(kL_p)^{-\alpha_1}\frac{k_i k_j}{k^2} + b(k)\left(\delta_{ij} - \frac{k_i k_j}{k^2}\right)\right]. \tag{A3}$$

Combining this expression with Eq. (37), one obtains

$$E_K(k) \approx \left(\frac{\nu_p}{\nu_f \tau_p}\right)^2 L_p^3\langle C_{mn}C_{mn}\rangle (kL_p)^{-\alpha_1-2}, \tag{A4}$$

and according to the observations, the power-law exponent is approximately -6, so that $\alpha_1 = 4$. We can decompose $\langle C_{mn}C_{mn}\rangle$ into "mean" and "fluctuating" contributions of $\boldsymbol{B} = \langle \boldsymbol{B}\rangle + \boldsymbol{B}'$:

$$\begin{aligned}\langle C_{mn}C_{mn}\rangle &= \langle B_{mi}B_{in}B_{mj}B_{jn}\rangle \\ &= \langle(\langle B_{mi}\rangle + B'_{mi})(\langle B_{in}\rangle + B'_{in})(\langle B_{mj}\rangle + B'_{mj})(\langle B_{jn}\rangle + B'_{jn})\rangle.\end{aligned} \tag{A5}$$

Assuming isotropy, Eq. (A5) simplifies to

$$\langle C_{mn}C_{mn}\rangle = \frac{1}{K_p^2}\left[\left(e_p^M\right)^2 + 6e_p^M e_p^F\right] + \langle B'_{mi}B'_{in}B'_{mj}B'_{jn}\rangle. \tag{A6}$$

The fourth-order correlation terms cannot be calculated directly and we approximated it assuming the fluctuation to be Gaussianly distributed, by

$$\langle B'_{mi}B'_{in}B'_{mj}B'_{jn}\rangle \approx \frac{3}{K_p^2}\left(e_p^F\right)^2. \tag{A7}$$

By combining the scaling in relation (A4) with (A6) and (A7), we have

$$E_K(k) \approx \left(\frac{L_p^3}{\nu_f^2}\right)\left[\left(e_p^M\right)^2 + 6e_p^M e_p^F + 3\left(e_p^F\right)^2\right](kL_p)^{-6} = \left(\frac{L_p^3}{\nu_f^2}\right)(Q_f)(kL_p)^{-6}, \tag{A8}$$

where the quantity $Q_f = (e_p^M)^2 + 6e_p^M e_p^F + 3(e_p^F)^2$.

APPENDIX B: DEMONSTRATION: $\sum_{k\in\mathbb{Z}} T_a(k) = 0$

In this Appendix, we will show the demonstration that the term $T_a(k)$ in Eq. (45) of Sec. V is a transfer term. The expression of $T_a^{\mathbf{k}}$ is

$$T_a^{\mathbf{k}} = 2K_p \mathrm{Re}(\widehat{\boldsymbol{A}\boldsymbol{B}}^{\mathbf{k}} : \overline{\widehat{\mathbf{B}}}^{\mathbf{k}}). \tag{B1}$$

We rewrite the terms using the Hermitian symmetry property $\overline{\widehat{\boldsymbol{B}}_{ij}}^{\mathbf{k}} = \widehat{\boldsymbol{B}}_{ij}^{-\mathbf{k}}$:

$$T_a^{\mathbf{k}} = 2K_p \mathrm{Re}\left(\overline{\widehat{B_{ij}}}^{\mathbf{k}} \sum_{\mathbf{p}+\mathbf{q}=\mathbf{k}} \widehat{A_{il}}^{\mathbf{p}}\widehat{B_{lj}}^{\mathbf{q}}\right) = 2K_p \mathrm{Re}\left(\widehat{B_{ij}}^{-\mathbf{k}} \sum_{\mathbf{p}+\mathbf{q}=\mathbf{k}} \widehat{A_{il}}^{\mathbf{p}}\widehat{B_{lj}}^{\mathbf{q}}\right). \tag{B2}$$

With change of variable $(-\mathbf{k}) \rightarrow \mathbf{k}$, we have

$$T_a^{\mathbf{k}} = 2K_p \mathrm{Re}\left(\sum_{\mathbf{p}+\mathbf{q}+\mathbf{k}=\mathbf{0}} \widehat{B_{ij}}^{\mathbf{k}} \widehat{A_{il}}^{\mathbf{p}} \widehat{B_{lj}}^{\mathbf{q}} \right)$$
$$= 2K_p \mathrm{Re}\left(\sum_{\mathbf{p}+\mathbf{q}+\mathbf{k}=\mathbf{0}} \widehat{B_{ij}}^{\mathbf{k}} \widehat{A_{il}}^{\mathbf{p}} \widehat{B_{lj}}^{\mathbf{q}} \right) = 2K_p \mathrm{Re}\left[\sum_{\mathbf{p}+\mathbf{q}+\mathbf{k}=\mathbf{0}} t_a(\mathbf{k},\mathbf{p},\mathbf{q}) \right].$$

We have decomposed the term $T_a^{\mathbf{k}}$ into a sum (integral) of more elementary terms $t_a(\mathbf{k},\mathbf{p},\mathbf{q}) = \widehat{B_{ij}}^{\mathbf{k}} \widehat{A_{il}}^{\mathbf{p}} \widehat{B_{lj}}^{\mathbf{q}}$. We can write $B_{ij} = B_{im}\delta_{mj} = B_{mi}\delta_{mj}$ because (B_{ij}) is symmetric matrix and $\widehat{A_{il}}^{\mathbf{p}} = -\widehat{A_{li}}^{\mathbf{p}}$ because (A_{ij}) is an antisymmetric matrix: $t_a(\mathbf{k},\mathbf{p},\mathbf{q}) = \delta_{mj} \widehat{B_{mi}}^{\mathbf{k}} \widehat{A_{il}}^{\mathbf{p}} \widehat{B_{lj}}^{\mathbf{q}}$. We can deduce

$$t_a(\mathbf{k},\mathbf{p},\mathbf{q}) = \widehat{B_{ij}}^{\mathbf{k}} \widehat{A_{il}}^{\mathbf{p}} \widehat{B_{lj}}^{\mathbf{q}} = \widehat{B_{ij}}^{\mathbf{k}} \left(-\widehat{A_{li}}^{\mathbf{p}}\right) \widehat{B_{ml}}^{\mathbf{q}} \delta_{mj} = -\delta_{mj} \widehat{B_{ml}}^{\mathbf{q}} \widehat{A_{li}}^{\mathbf{p}} \widehat{B_{ij}}^{\mathbf{k}} \tag{B3}$$
$$= -t_a(\mathbf{q},\mathbf{p},\mathbf{k}). \tag{B4}$$

Finally, if we sum all the triads, we deduce

$$\sum_{k\in\mathbb{Z}} T_a(k) = 2K_p \sum_{k\in\mathbb{Z}} \sum_{|\boldsymbol{k}|=k} \left\{ \mathrm{Re}\left[\sum_{\mathbf{p}+\mathbf{q}+\mathbf{k}=\mathbf{0}} t_a(\mathbf{k},\mathbf{p},\mathbf{q}) \right] \right\} = 0 \tag{B5}$$

because the summation involves all triads, for each given triad $t_a(\mathbf{k},\mathbf{p},\mathbf{q})$ we can find an opposite triad $t_a(\mathbf{q},\mathbf{p},\mathbf{k}) = -t_a(\mathbf{k},\mathbf{p},\mathbf{q})$, so the integral sums up to zero.

APPENDIX C: DETAILS OF THE NONLOCAL TRIAD INTERACTION BEHIND THE POLYMER-FLUID TRANSFER TERM

In this Appendix, we will show the detailed demonstration in order to prove the term $T_S(k)$ in Eq. (50) of Sec. V C is a transfer term. This term is the combination of the action of fluid flow on the polymer $S_{f\rightarrow p}(k)$, and the back-reaction of the polymer on the flow $S_{p\rightarrow f}(k)$. We need to demonstrate $\sum_{k\in\mathbb{Z}} S_{p\rightarrow f}(k) + S_{f\rightarrow p}(k) = 0$. We can compute $S_{f\rightarrow p}(k)$ and $S_{p\rightarrow f}(k)$ by relation

$$S_{f\rightarrow p}(k) = \sum_{|\boldsymbol{k}|=k} S_{f\rightarrow p}^{\mathbf{k}} \quad \text{and} \quad S_{p\rightarrow f}(k) = \sum_{|\boldsymbol{k}|=k} S_{p\rightarrow f}^{\mathbf{k}}, \tag{C1}$$

where

$$S_{f\rightarrow p}^{\mathbf{k}} = 2K_p \mathrm{Re}(\widehat{\boldsymbol{B}\cdot\nabla\boldsymbol{u}}^{\boldsymbol{k}} : \widehat{\overline{\boldsymbol{B}}}^{\boldsymbol{k}}) = 2K_p \mathrm{Re}\left(\sum_{\mathbf{p}+\mathbf{q}=\mathbf{k}} \widehat{B_{im}}^{\mathbf{p}} \underline{i} q_m \widehat{u_j}^{\mathbf{q}} \widehat{\overline{B}}_{ij}^{\mathbf{k}} \right), \tag{C2}$$

$$S_{p\rightarrow f}^{\mathbf{k}} = \frac{\nu_p}{\tau_p} \mathrm{Re}[\nabla \cdot \widehat{(\boldsymbol{B}\cdot\boldsymbol{B})}^{\boldsymbol{k}} \cdot (\widehat{\overline{\boldsymbol{u}}})^{\boldsymbol{k}}] = \frac{\nu_p}{\tau_p} \mathrm{Re}\left(\sum_{\mathbf{p}+\mathbf{q}=\mathbf{k}} \underline{i} k_j \widehat{B}_{im}^{\mathbf{p}} \widehat{B}_{mj}^{\mathbf{q}} \widehat{\overline{u}_i}^{\mathbf{k}} \right), \tag{C3}$$

where $2K_p = \frac{\nu_p}{\tau_p}$ as in Appendix B and the bars $\widehat{\overline{u}_i}$ and $\widehat{\overline{B}_{ij}}$ represent the complex conjugate of $\widehat{u}_i$ and $\widehat{B}_{ij}$, respectively. We consider for this derivation the assumption of weak stretching $(L_{\max}^2) \gg \langle C_{ii} \rangle$, so that we can neglect Peterlin's correction and therefore $\mathcal{P} \approx 1$.

We rewrite these two terms by using the Hermitian symmetry property $\widehat{\overline{B_{ij}}}^{\mathbf{k}} = \widehat{B}_{ij}^{-\mathbf{k}}$ and $\widehat{\overline{u_i}}^{\mathbf{k}} = \widehat{u}_i^{(-\mathbf{k})}$, and at the same time, changing the variable $-\boldsymbol{k}$ into $\boldsymbol{k}$, we obtain

$$S_{f\to p}^{\mathbf{k}} = 2K_p \mathrm{Re}\left(\sum_{\mathbf{p}+\mathbf{q}+\mathbf{k}=\mathbf{0}} \widehat{B_{im}}^{\mathbf{p}}\, \underline{i}\, q_m\, \widehat{u_j}^{\mathbf{q}}\, \widehat{B}_{ij}^{\mathbf{k}} \right) = 2K_p \mathrm{Re}\left[\sum_{\mathbf{p}+\mathbf{q}+\mathbf{k}=\mathbf{0}} t_{f\to p}(\mathbf{k},\mathbf{p},\mathbf{q}) \right], \tag{C4}$$

$$S_{p\to f}^{\mathbf{k}} = \frac{\nu_p}{\tau_p} \mathrm{Re}\left(\sum_{\mathbf{p}+\mathbf{q}+\mathbf{k}=\mathbf{0}} \underline{i}\, k_j\, \widehat{B}_{im}^{\mathbf{p}}\, \widehat{B}_{mj}^{\mathbf{q}}\, \widehat{u_i}^{\mathbf{k}} \right) = \frac{\nu_p}{\tau_p} \mathrm{Re}\left[\sum_{\mathbf{p}+\mathbf{q}+\mathbf{k}=\mathbf{0}} t_{p\to f}(\mathbf{k},\mathbf{p},\mathbf{q}) \right] \tag{C5}$$

with $t_{f\to p}(\mathbf{k},\mathbf{p},\mathbf{q}) = \widehat{B}_{ij}^{\mathbf{k}}\, \widehat{B}_{im}^{\mathbf{p}}\, \underline{i}\, q_m\, \widehat{u}_j^{\mathbf{q}}$ and $t_{p\to f}(\mathbf{k},\mathbf{p},\mathbf{q}) = -\widehat{B}_{im}^{\mathbf{p}}\, \widehat{B}_{mj}^{\mathbf{q}}\, \underline{i} k_j\, \widehat{u}_i^{\mathbf{k}}$.

Using that $\widehat{B}_{ij}^{\mathbf{k}} = \widehat{B}_{im}^{\mathbf{k}} \delta_{mj}$, we have $t_{f\to p}(\mathbf{k},\mathbf{p},\mathbf{q}) = (\widehat{B}_{im}^{\mathbf{k}}\, \widehat{B}_{im}^{\mathbf{p}}\, \underline{i}\, q_m\, \widehat{u}_j^{\mathbf{q}})\, \delta_{mj}$. Since $\boldsymbol{B}$ is a symmetric matrix $\widehat{B}_{im}^{\mathbf{k}} = \widehat{B}_{mi}^{\mathbf{k}}$ we have

$$t_{f\to p}(\mathbf{k},\mathbf{p},\mathbf{q}) = \left(\widehat{B}_{mi}^{\mathbf{k}}\, \widehat{B}_{im}^{\mathbf{p}}\, \underline{i}\, q_m\, \widehat{u}_j^{\mathbf{q}}\right)\delta_{mj}. \tag{C6}$$

We can write $\widehat{u}_i^{\mathbf{k}} = \widehat{u}_m^{\mathbf{k}} \delta_{mi}$, and we have

$$t_{p\to f}(\mathbf{k},\mathbf{p},\mathbf{q}) = -\left(\widehat{B}_{il}^{\mathbf{p}}\, \widehat{B}_{lj}^{\mathbf{q}}\, \underline{i}\, k_j\, \widehat{u}_m^{\mathbf{k}}\right)\, \delta_{mi}. \tag{C7}$$

Thus, when we compare (C7) and (C6), we obtain

$$t_{f\to p}(\mathbf{k},\mathbf{p},\mathbf{q}) = -t_{p\to f}(\mathbf{p},\mathbf{q},\mathbf{k}). \tag{C8}$$

Finally, if we sum all the triads we deduce

$$\sum_{k\in\mathbb{Z}} S_{p\to f}(k) + S_{f\to p}(k) = \sum_{k\in\mathbb{Z}} \sum_{|\boldsymbol{k}|=k} \frac{\nu_p}{\tau_p} \left\{ \mathrm{Re}\left[\sum_{\mathbf{p}+\mathbf{q}+\mathbf{k}=\mathbf{0}} t_{f\to p}(\mathbf{k},\mathbf{p},\mathbf{q}) + t_{p\to f}(\mathbf{k},\mathbf{p},\mathbf{q}) \right] \right\} = 0 \tag{C9}$$

by using $2K_p = \nu_p/\tau_p$ and because the summation involves all triads, for any given triad $t_{f\to p}(\mathbf{k},\mathbf{p},\mathbf{q})$, we can find a triad having opposite value $t_{p\to f}(\mathbf{p},\mathbf{q},\mathbf{k})$ and inversely. So, the integral is equal to zero, and $\sum_{k\in\mathbb{Z}} T_S(k) = 0$.

The final result

$$\sum_{k\in\mathbb{Z}} S_{p\to f}(k) + S_{f\to p}(k) = 0 \tag{C10}$$

means that globally these terms transfer the energy between polymer and fluid. Reference [43] demonstrates this by using physical space arguments.

APPENDIX D: INFLUENCE OF ARTIFICAL DIFFUSIVITY ON THE ENERGY SPECTRA

As we can see in Fig. 6, the artificial diffusivity ν_a is chosen small enough to ensure the corresponding term in Lin's equation not to become dominant in the wave number range we focus on. In order to compare the effect of artificial diffusivity, and to check if the value we chose is low enough, we repeated case a3 with two different values of ν_a: case a3-0 with $\nu_a = 0$ (artificial diffusivity free) and case a3-1 with $\frac{\nu_f}{\nu_a} = 625$ (double artificial diffusivity). The case a3 is the only case allowing us to simulate with zero artificial diffusivity. The other cases suffer numerical instability in the absence of numerical diffusivity. We observe in Fig. 8 that the artificial diffusivity can affect the power law observed well before the Batchelor scale. This illustrates the importance to use a method where the numerical diffusivity can be chosen as small as possible, as in the present approach.

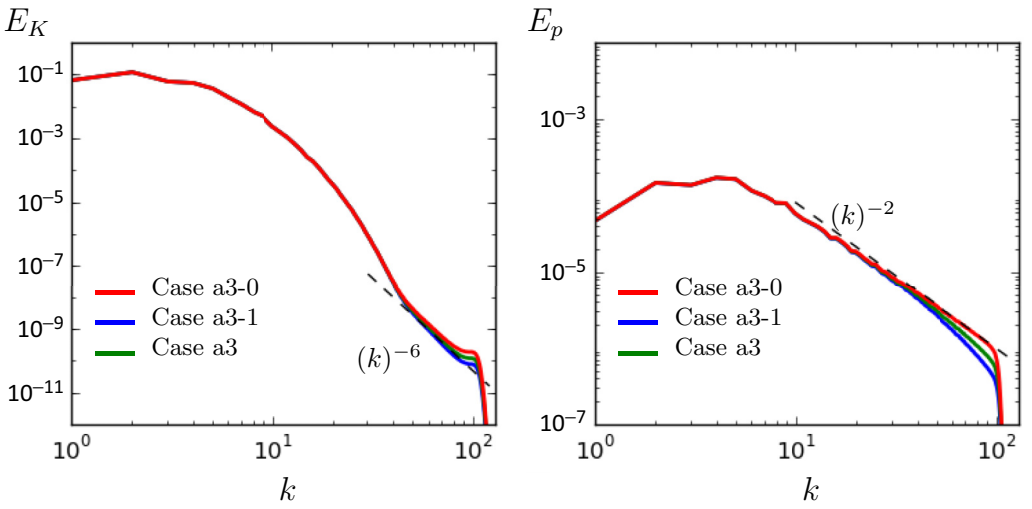

FIG. 8. Assessment of the effect of artificial diffusivity ν_a on the kinetic and polymer energy spectra.

[1] B. A. Toms, Some observation on the flow of linear polymer solutions through straight tubes at large reynolds numbers, in *Proceedings of the 1st International Congress on Rheology* (North Holland, Amsterdam, 1949), Vol. II, pp. 135–141.

[2] P. S. Virk, Drag reduction fundamentals, AIChE J. **21**, 625 (1975).

[3] P. S. Virk, D. C. Sherman, and D. L. Wagger, Additive equivalence during turbulent drag reduction, AIChE J. **43**, 3257 (1997).

[4] C. M. White and M. G. Mungal, Mechanics and prediction of turbulent drag reduction with polymer additives, Annu. Rev. Fluid Mech. **40**, 235 (2008).

[5] J. Lumley, Drag reduction by additives, Annu. Rev. Fluid Mech. **1**, 367 (1969).

[6] M. Tabor and P. G. de Gennes, A cascade theory of drag reduction, Europhys. Lett. **2**, 519 (1986).

[7] P. De Gennes, *Introduction to Polymer Dynamics* (Cambridge University Press, Cambridge, 1990).

[8] P. De Gennes, Towards a scaling theory of drag reduction, Phys. A (Amsterdam) **140**, 9 (1986).

[9] I. Procaccia, V. S. L'vov, and R. Benzi, Colloquium : Theory of drag reduction by polymers in wall-bounded turbulence, Rev. Mod. Phys. **80**, 225 (2008).

[10] Y. Dubief, C. M. White, V. E. Terrapon, E. S. Shaqfeh, P. Moin, and S. K. Lele, On the coherent drag-reducing turbulence enhancing behavior of polymers in wall flows, J. Fluid Mech. **514**, 271 (2004).

[11] Y. Dubief, V. Terrapon, C. White, E. Shaqfeh, P. Moin, and S. Lele, New answers on the interaction between polymers and vortices in turbulent flows, Flow Turbul. Combust. **74**, 311 (2005).

[12] T. Vaithianathan, A. Robert, J. G. Brasseur, and L. R. Collins, Polymer mixing in shear-driven turbulence, J. Fluid Mech. **585**, 487 (2007).

[13] P. Perlekar, D. Mitra, and R. Pandit, Direct numerical simulations of statistically steady, homogeneous, isotropic fluid turbulence with polymer additives, Phys. Rev. E **82**, 066313 (2010).

[14] W. K. A. Liberzon, M. Guala, and A. Tsinober, On turbulent kinetic energy production and dissipation in dilute polymer solutions, Phys. Fluids **18**, 125101 (2006).

[15] D. Bonn, Y. Couder, P. H. J. van Dam, and S. Douady, From small scales to large scales in three-dimensional turbulence: The effect of diluted polymers, Phys. Rev. E **47**, R28 (1993).

[16] T. Watanabe and T. Gotoh, Coil-stretch transition in an ensemble of polymers in isotropic turbulence, Phys. Rev. E **81**, 066301 (2010).

[17] A. Gupta, P. Perlekar, and R. Pandit, Two-dimensional homogeneous isotropic fluid turbulence with polymer additives, Phys. Rev. E **91**, 033013 (2015).

[18] V. E. Terrapon, Y. Dubief, P. Moin, E. S. G. Shaqfeh, and S. K. Lele, Simulated polymer stretch in a turbulent flow using brownian dynamics, J. Fluid Mech. **504**, 61 (2004).
[19] R. Benzi, E. De Angelis, R. Govindarajan, and I. Procaccia, Shell model for drag reduction with polymer additives in homogeneous turbulence, Phys. Rev. E **68**, 016308 (2003).
[20] R. Benzi, E. S. C. Ching, and I. Procaccia, Drag reduction in homogeneous turbulence by scale-dependent effective viscosity, Phys. Rev. E **70**, 026304 (2004).
[21] K. Kim, C. F. Li, R. Sureshkumar, S. Balachandar, and R. J. Adrian, Effects of polymer stresses on eddy structures in drag-reduced turbulent channel flow, J. Fluid Mech. **584**, 281 (2007).
[22] A. Robert, T. Vaithianathan, L. R. Collins, and J. G. Brasseur, Polymer-laden homogeneous shear-driven turbulent flow: A model for polymer drag reduction, J. Fluid Mech. **657**, 189 (2010)
[23] M. D. Warholic, H. Massah, and T. J. Hanratty, Influence of drag-reducing polymers on turbulence: Effects of Reynolds number, concentration and mixing, Exp. Fluids **27**, 461 (1999).
[24] P. K. Ptasinski, F. T. M. Nieuwstadt, B. H. A. A. van den Brule, and M. Hulsen, Experiments in turbulent pipe flow with polymer additives at maximum drag reduction, Flow, Turbul. Combust **66**, 159 (2001).
[25] T. Vaithianathan and L. R. Collins, Numerical approach to simulating turbulent flow of a viscoelastic polymer solution, J. Comput. Phys. **187**, 1 (2003).
[26] C. M. Casciola and E. De Angelis, Energy transfer in turbulent polymer solutions, J. Fluid Mech. **581**, 419 (2007).
[27] R. Benzi, E. DeAngelis, V. L'vov, and I. Procaccia, Identification and Calculation of the Universal Asymptote for Drag Reduction by Polymers in Wall Bounded Turbulence, Phys. Rev. Lett. **95**, 194502 (2005).
[28] P. C. Valente, C. B. da Silva, and F. T. Pinho, The effect of viscoelasticity on the turbulent kinetic energy cascade, J. Fluid Mech. **760**, 39 (2014).
[29] H. Xi, E. Bodenschatz, and H. Xu, Elastic Energy Flux by Flexible Polymers in Fluid Turbulence, Phys. Rev. Lett. **111**, 024501 (2013).
[30] A. Groisman and V. Steinberg, Elastic turbulence in a polymer solution flow, Nature (London) **405**, 53 (2000).
[31] A. Groisman and V. Steinberg, Efficient mixing at low Reynolds numbers using polymer additives, Nature (London) **410**, 905 (2001).
[32] T. Burghelea, E. Segre, and V. Steinberg, Elastic turbulence in Von Karman swirling flow between two disks, Phys. Fluids **19**, 053104 (2007).
[33] S. Berti, A. Bistagnino, G. Boffetta, A. Celani, and S. Musacchio, Two-dimensional elastic turbulence, Phys. Rev. E **77**, 055306 (2008).
[34] A. Fouxon and V. Lebedev, Spectra of turbulence in dilute polymer solutions, Phys. Fluids **15**, 2060 (2003).
[35] D. Samanta, Y. Dubief, M. Holzner, C. Schäfer, A. N. Morozov, C. Wagner, and B. Hof, Elasto-inertial turbulence, Proc. Natl. Acad. Sci. USA **110**, 10557 (2013).
[36] Y. Dubief, V. E. Terrapon, and J. Soria, On the mechanism of elasto-inertial turbulence, Phys. Fluids **25**, 110817, (2013).
[37] V. E. Terrapon, Y. Dubief, and J. Soria, On the role of pressure in elasto-inertial turbulence, J. Turbul. **16**, 26 (2015).
[38] L. Thais, G. Mompean, and T. B. Gatski, Spectral analysis of turbulent viscoelastic and Newtonian channel flows, J. Non-Newtonian Fluid Mech. **200**, 165 (2013).
[39] T. Watanabe and T. Gotoh, Hybrid Eulerian–Lagrangian simulations for polymer–turbulence interactions, J. Fluid Mech. **717**, 535 (2013).
[40] T. Watanabe and T. Gotoh, Power-law spectra formed by stretching polymers in decaying isotropic turbulence, Phys. Fluids **26**, 035110 (2014).
[41] N. Balci, B. Thomases, M. Renardy, and C. Doering, Symmetric factorization of the conformation tensor in viscoelastic fluid models, J. Non-Newtonian Fluid Mech. **166**, 546 (2011).
[42] A. Peterlin, Hydrodynamics of macromolecules in a velocity field with longitudinal gradient, J. Polym. Sci., Part B: Polym. Phys. **4**, 287 (1966).

[43] E. De Angelis, C. M. Casciola, and R. Piva, Energy spectra in viscoelastic turbulence, Phys. D (Amsterdam) **241**, 297 (2012); special Issue on Small Scale Turbulence.
[44] R. Bird, R. Armstrong, and O. Hassager, *Dynamics of Polymeric liquids*, Fluid Mechanics, Vol. 1, 2nd ed. (Wiley, New York, 1987).
[45] R. Sureshkumar and N. Beris, Effect of artificial stress diffusivity on the stability of numerical calculations and the flow dynamics of time-dependent viscoelastic flows, J. Non-Newtonian Fluid Mech. **60**, 53 (1995).
[46] R. Sureshkumar, A. N. Beris, and R. A. Handler, Direct numerical simulation of the turbulent channel flow of a polymer solution, Phys. Fluids **9**, 743 (1997).
[47] P. Stewart, N. Lay, M. Sussman, and M. Ohta, An improved sharp interface method for viscoelastic and viscous two-phase flows, J. Sci. Comput. **35**, 43 (2008).
[48] R. Fattal and R. Kupferman, Time-dependent simulation of viscoelastic flows at high Weissenberg number using the log-conformation representation, J. Non-Newtonian Fluid Mech. **126**, 23 (2005).
[49] X. Chen, H. Marschall, M. Schäfer, and D. Bothe, A comparison of stabilisation approaches for finite-volume simulation of viscoelastic fluid flow, Int. J. Comput. Fluid Dyn. **27**, 229 (2013).
[50] L. Thais, T. B. Gatski, and G. Mompean, Some dynamical features of the turbulent flow of a viscoelastic fluid for reduced drag, J. Turb. (13), **N19** (2012).
[51] S. Chen, G. D. Doolen, R. H. Kraichnan, and Z.-S. She, On statistical correlations between velocity increments and locally averaged dissipation in homogeneous turbulence, Phys. Fluids **5**, 458 (1993).
[52] P. D. Mininni, D. Rosenberg, and A. Pouquet, Isotropization at small scales of rotating helically driven turbulence, J. Fluid Mech. **699**, 263 (2012).
[53] C. Canuto, M. Y. Hussaini, A. Quarteroni, and T. A. Zang, *Spectral Methods: Evolution to Complex Geometries and Applications to Fluid Dynamics* (Springer, London, 2007).
[54] T. Y. Hou and R. Li, Computing nearly singular solutions using pseudo-spectral methods, J. Comput. Phys. **226**, 379 (2007).